Structures of Ser205 mutant plasmepsin II from *Plasmodium falciparum* at 1.8 Å in complex with the inhibitors rs367 and rs370

**Oluwatoyin A. Asojo,* Elena
Afonina, Sergei V. Gulnik,
Betty Yu, John W. Erickson,
Ramnarayan Randad, Djamel
Medjahed and Abelardo M. Silva**

Structure Biochemistry Program, National
Cancer Institute/SAIC, Frederick, MD 21702,
USA

Correspondence e-mail: asojo@ncifcrf.gov

Plasmepsin II is one of the four catalytically active plasmepsins found in the food vacuole of *Plasmodium falciparum*. These enzymes initiate hemoglobin degradation by cleavage at the α-chain between Phe33 and Leu34. The crystal structures of Ser205 mutant plasmepsin II from *P. falciparum* in complex with two inhibitors have been refined at a resolution of 1.8 Å in the space group *I*222 and to *R* factors of 19.9 and 19.5%. Each crystal contains one monomer in the asymmetric unit. Both inhibitors have a Phe–Leu core and incorporate tetrahedral transition-state mimetic hydroxypropylamine. The inhibitor rs367 possesses a 2,6-dimethylphenyloxyacetyl group at the P2 position and 3-aminobenzamide at the P2′ position, while rs370 has the same P2 group but 4-aminobenzamide in the P2′ position. These complexes reveal key conserved hydrogen bonds between the inhibitor and the binding-cavity residues, notably with the flap residues Val78 and Ser79, the catalytic dyad Asp34 and Asp214 and the residues Ser218 and Gly36 that are in proximity to the catalytic dyad. The structures also show unexpected conformational variability of the binding cavity of plasmepsin II and may reflect the mode of binding of the hemoglobin α-chain for cleavage.

1. Introduction

Plasmepsin II, the first protein from a protozoan parasite of the genus *Plasmodium* for which the structure was determined, is an aspartic protease involved in hemoglobin degradation (Silva *et al.*, 1996). Different species of *Plasmodium* are the etiologic agents of malaria, a devastating human disease afflicting several hundred million people a year and killing an estimated two million of them, mostly children (World Health Organization, 1995). *Plasmodium* species, such as *P. falciparum* and *P. vivax*, cause disease in the intra-erythrocytic phase of malaria. During this phase, the parasite consumes nearly all the host's hemoglobin to generate amino acids for its growth and maturation (Francis *et al.*, 1997). This is a vast catabolic process, since hemoglobin constitutes 95% of the soluble erythrocytic protein.

Hemoglobin is degraded by a series of proteases in an acidic digestive vacuole. This sequential process is initiated by aspartic proteases called plasmepsins. Two such homologous enzymes termed plasmepsin I and II (PLM I and PLM II) make an initial attack on the hemoglobin α-chain between residues 33 and 34. This initial attack is followed by cleavage by the cysteine protease falcipain, which allows further degradation of hemoglobin by other proteases in the food vacuole. The products of digestive-vacuole proteolysis are

Table 1
Statistics for data collection and model refinement.

Values in parentheses are for the highest resolution shell.

Data	Plm II–rs367	Plm II–rs370
All data		
Resolution (Å)	20–1.8 (1.9–1.8)	20–1.8 (1.9–1.8)
R_{merge}† (%)	6.0 (19.0)	5.8 (25.0)
Completeness (%)	71 (33)	95 (53)
Total No. of unique reflections	26322	35627
Redundancy	4.0 (3.0)	4.0 (3.0)
$I/\sigma(I)$	13.1(2.0)	15.0 (3.0)
Refinement [$I > 2\sigma(I)$]		
Resolution (Å)	20–1.8 (1.9–1.8)	20–1.8 (1.9–1.8)
R factor‡ (%)	19.9 (26.4)	19.5 (26.7)
R_{free}§ (%)	26.6 (29.6)	25.8 (28.7)
Geometry		
R.m.s. deviations		
Bond length (Å)	0.019	0.017
Bond angles (°)	2.1	2.1
Improper angles (°)	1.8	1.6
Dihedral angles (°)	27.5	27.4
Mean B factor (Å²)	36.7	35.4
Model information		
Mutant	Ser205	Ser205
Number of monomers	1	1
Per monomer		
No. of residues	331	331
No. of inhibitors	1	1
No. of waters	339	339

† $R_{merge} = \sum |I - \langle I \rangle|/\sum I$, where I is the observed intensity and $\langle I \rangle$ is the average intensity obtained from multiple observations of symmetry-related reflections after rejections. ‡ R factor $= \sum |F_o - |F_c||/\sum |F_o|$, where F_o are observed and F_c are calculated structure factors. § R_{free} set uses 5% of randomly chosen reflections defined in Brünger (1992a).

small peptides, which appear to be exported for terminal degradation by cytoplasmic exopeptidases (Goldberg *et al.*, 1991; Gluzman *et al.*, 1994; Dame *et al.*, 1994; Francis *et al.*, 1994). Intact hemoglobin cannot be cleaved by falcipain unless the substrate is first denatured (Francis *et al.*, 1996). Cysteine protease inhibitors cause osmotic swelling of the digestive vacuole and ultimately result in the death of the parasite (Rosenthal *et al.*, 1991). This may occur through the accumulation of digestion products that are too large to exit the vacuole (Francis *et al.*, 1996).

Both PLM I and PLM II are capable of making an initial cleavage in the hemoglobin α-chain between Phe33 and Leu34 (Gluzman *et al.*, 1994; Goldberg *et al.*, 1991). This bond is also the first to be cleaved when hemoglobin is incubated with an extract of purified digestive vacuoles (Goldberg *et al.*, 1991). This cleavage leads to unraveling of the hemoglobin molecule, allowing further proteolysis to proceed efficiently. The plasmepsins are capable of several other cleavages after the initial event (Gluzman *et al.*, 1994).

Of the ten plasmepsins that have been identified in the genome of *P. falciparum*, only four of them are active in the food vacuole during the intra-erythrocytic stage. These four are PLM I, PLM II, PLM IV and HAP, an aspartic protease with histidine in the active site (Banerjee *et al.*, 2002). PLM I and PLM II are 73% identical to each other, while their mature coding regions share about 64% identity with PLM IV and 60% identity with HAP, but only about 30–35% identity

with mammalian aspartic proteases such as cathepsin D (Francis *et al.*, 1994).

The structures of PLM II from *P. falciparum* in complex with pepstatin A (Silva *et al.*, 1996), plasmepsin from *P. vivax* in complex with pepstatin A and N-truncated pro-PLM II from *P. falciparum* (Bernstein *et al.*, 1999) have been determined by X-ray crystallographic techniques. All three sets of coordinates have been deposited in the RSCB Protein Data Bank with accession codes 1sme, 1qs8 and 1pfs, respectively.

Inhibitors of PLM II that have low nanomolar inhibition constant values and are lethal against cultured malarial parasites have been identified (Carroll, Johnson *et al.*, 1998; Carroll & Orlowski, 1998; Carroll, Patel *et al.*, 1998; Goldberg, 1992; Goldberg *et al.*, 1991; Haque *et al.*, 1999; Silva *et al.*, 1996, 1998; Westling *et al.*, 1999). Furthermore, some aspartic and cysteine protease inhibitors demonstrate an apparent synergistic inhibition of hemoglobin degradation in both culture and a murine malaria model (Semenov *et al.*, 1998). Thus, aspartyl and cysteine protease inhibitors could provide an array of new antimalarial drugs to confront the problems of widespread drug resistance facing the current therapeutics. We present here the structures of complexes of PLM II from *P. falciparum* with new inhibitors. Since the inhibitors have a Phe–Leu core, they provide a view of the possible conformation of the enzyme when the natural substrate hemoglobin is bound.

2. Experimental

2.1. Purification and crystallization of PLM II with rs367 and rs370

The expression and purification of PLM II was carried out as described previously (Gulnik *et al.*, 2002). Solvent-exposed Met205 was substituted with Ser, which is less tolerated in the hydrophobic S1 subsite of the enzyme and thus reduces the chances of autolysis of the protein during purification. The mutant enzyme retained its full catalytic activity. Protein from the Ser205 mutant, rather than the wild type, was used for crystallographic experiments (Gulnik *et al.*, 2002).

The crystals were grown at 293 K by vapor diffusion in hanging drops. Drops were prepared by mixing 2 µl of protein–inhibitor solution with an equal volume of the appropriate reservoir solution. The protein–inhibitor solution was comprised of 5 mg ml⁻¹ protein in 10 m*M* Tris–HCl pH 7.0 and 7 m*M* inhibitor in 10% DMSO. The reservoir solutions for the complexes of PLM II with both rs367 and rs370 contained 0.10 *M* sodium citrate buffer pH 6.0, 0.20 *M* phosphate buffer, 18% $(NH_4)_2SO_4$ and 5% ethanol. Large well ordered crystals grew in several days.

2.2. Data collection

Crystals were transferred into a cryoprotectant mother liquor containing 25% glycerol prior to flash-freezing at 100 K in a stream of N_2 gas. Crystals of both the PLM II–rs367 and PLM II–rs370 complexes diffracted to about 1.8 Å resolution. These orthorhombic crystals belonged to the space group *I*222 and have similar unit-cell parameters: a = 76.0, b = 85.5,

$c = 123.4$ Å for the former and $a = 75.9$, $b = 84.8$, $c = 123.4$ Å for the latter. Both data sets were collected at beamline X9B at Brookhaven National Synchrotron Light Source using a MAR 345 detector (MAR Research). X-ray data sets were processed using the programs *DENZO* (Otwinowski, 1993*a*) and *SCALEPACK* (Otwinowski, 1993*b*).

2.3. Refinement

The structures were solved by molecular replacement using the program *AMoRe* (Navaza, 1994). The search model was obtained by stripping a monomer from the 2.7 Å structure of PLM II complexed with pepstatin A of its ligand and water molecules (Silva *et al.*, 1996). The initial *R* factors of the unrefined solution from *AMoRe* were 34% (free *R* factor 42%) and 32% (free *R* factor 40%) for the PLM II–rs367 and

(a)

(b)

Figure 1
Fit of the structural models in the vicinity of the inhibitors (*a*) rs367 and (*b*) rs370 in the final respective $2F_o - F_c$ electron-density maps, contoured at 1.5σ. Note that the water molecule that assumes alternate positions depending on the position of the amine group at the P2′ position of the inhibitor has well ordered electron density.

PLM II–rs370 complexes, respectively. Iterative cycles of model building into the $2F_o - F_c$ omit electron-density maps with the program *O* (Jones *et al.*, 1991) and structure refinement were carried out. The models were refined to 2.0 Å using both positional refinement and simulated annealing with *X-PLOR* (Adams *et al.*, 1997; Brünger, 1992*a,b*; Brunger *et al.*, 1997, 1990). This was followed with refinement cycles to the full resolution limit of 1.8 Å with the *CNS* maximum-likelihood refinement procedure using Engh and Huber geometric parameters (Adams *et al.*, 1997; Brünger, 1992*a,b*; Brünger *et al.*, 1997, 1990). The refined models each include one protein molecule and one inhibitor molecule as well as 339 water molecules, with *R* factors of 19.9% (free *R* factor 26.6%) and 19.5% (free *R* factor 25.8%) for the complexes with rs367 and rs370, respectively. The data and model statistics are summarized in Table 1.
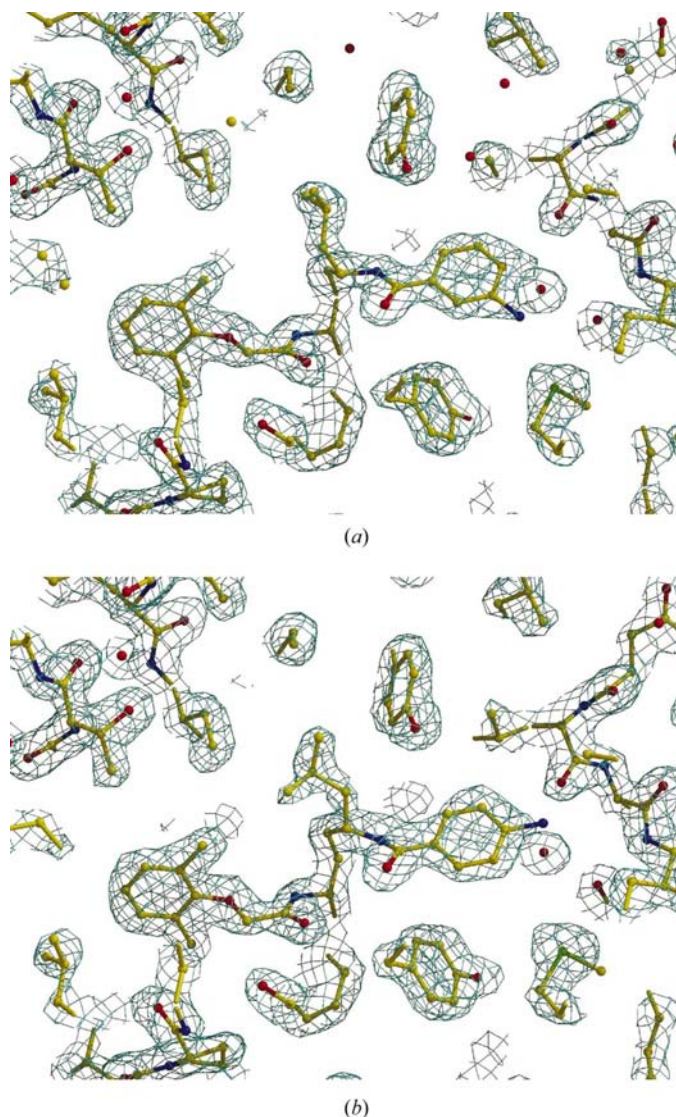
3. Results and discussion

3.1. Quality of the models

The quality of the final models is summarized in Table 1. The stereochemical quality of the structures as assessed by *PROCHECK* (Laskowski *et al.*, 1993) are excellent and all main-chain and side-chain parameters are either better than or as expected for 1.8 Å structures. The Ramanchandran plot for the PLM II–rs367 complex shows that only 1.4% of the residues are in the disallowed regions, with all the rest lying in the allowed regions; for PLM II–rs370 only 1.7% lie in the disallowed region. All main-chain and side-chain atoms fit well into the $2F_o - F_c$ electron-density map. Examples of the quality of these maps are shown in Fig. 1.

3.2. Complexes of PLM II with rs370/rs367

As part of our HIV protease-inhibitor program, we designed and synthesized inhibitors that incorporate a symmetry-based transition-state mimetic hydroxypropyl amine (Phe–Phe) isostere. These retroviral aspartic protease inhibitors were screened against PLM II. The results were encouraging since several non-peptidic small-molecular-weight P2–P2′ compounds exhibited submicromolar inhibition constants against PLM II.

In an attempt to further improve potency, we turned our attention to the initial Phe–Leu cleavage-site region in the hemoglobin α-chain. On the basis of the above substrate specificity, we designed a Phe–Leu core incorporating tetrahedral transition-state mimetic hydroxypropylamine. We were able to co-crystallize PLMII with two of these inhibitors. The two inhibitors are 3-amino-*N*-{4(2,6-dimethyl-phenoxy)-acetylamino]-3-hydroxy-1-isobutyl-5-phenyl-pentyl}-benzamide, otherwise known as rs367, and 4-amino-*N*-{4(2,6-di-methyl-phenoxy)-acetylamino]-3-hydroxy-1-isobutyl-5-phenyl-pentyl}-benzamide, referred to as rs370. The structural formulae are shown in Fig. 2. Rs367, possessing a 2,6-di-methylphenyloxyacetyl group at the P2 position and a 3-aminobenzamide at the P2′ position, exhibited a PLM II inhibition K_i of about an order of magnitude better than the

corresponding inhibitors possessing a Phe–Phe core. There is negligible difference in the inhibition-constant values of both rs367 and rs370 against PLM II, with inhibition-constant values of 18 nM for the former and 30 nM for the latter. Further modification to the P2′ position provided other analogs with low nanomolar potency, thus establishing the Phe–Leu derivatives as an interesting series of lead inhibitors. Data from an extensive inhibitor study will be published elsewhere (Gulnik *et al.*, unpublished results).

3.3. General features of the models

PLM II displays the characteristic folding of eukaryotic aspartic proteases which has been observed from mammalian enzymes such as human pepsin, renin, gastricsin and cathepsin D to the fungal enzymes endothiapepsin and rizopuspepsin. The main secondary-structure features of PLM II are retained regardless of which inhibitor is bound. The molecule is formed by a single chain of 329 amino acids and is folded into two topologically similar N- and C-terminal domains. The domains contact each other along the bottom of the binding cleft that contains the catalytic dyad, Asp34 and Asp214. A single-hairpin structure, known as the 'flap', lies perpendicular over the binding cleft and interacts with bound inhibitors and presumably substrates. The amino and carboxyl ends of the polypeptide chain of PLM II are assembled into a characteristic six-stranded interdomain β-sheet, which serves to anchor the domains together (Fig. 3a).

The structures of the PLM II–rs367 and PLM II–rs370 complexes are virtually identical except for the difference in the position of the amino groups in the P2′ inhibitors. The
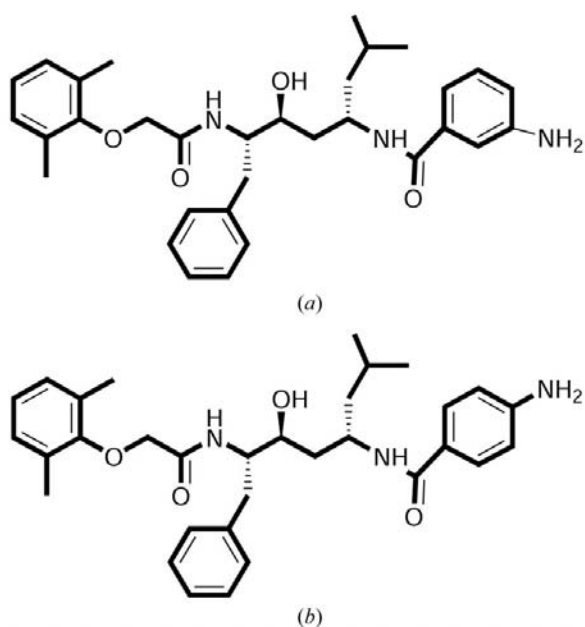
r.m.s. deviation on overlapping the main-chain atoms of the two models is 0.201 Å. The r.m.s. deviations were calculated using the program *LSQKAB* (Kabsch, 1976) within the *CCP*4 package (Collaborative Computational Project, Number 4,
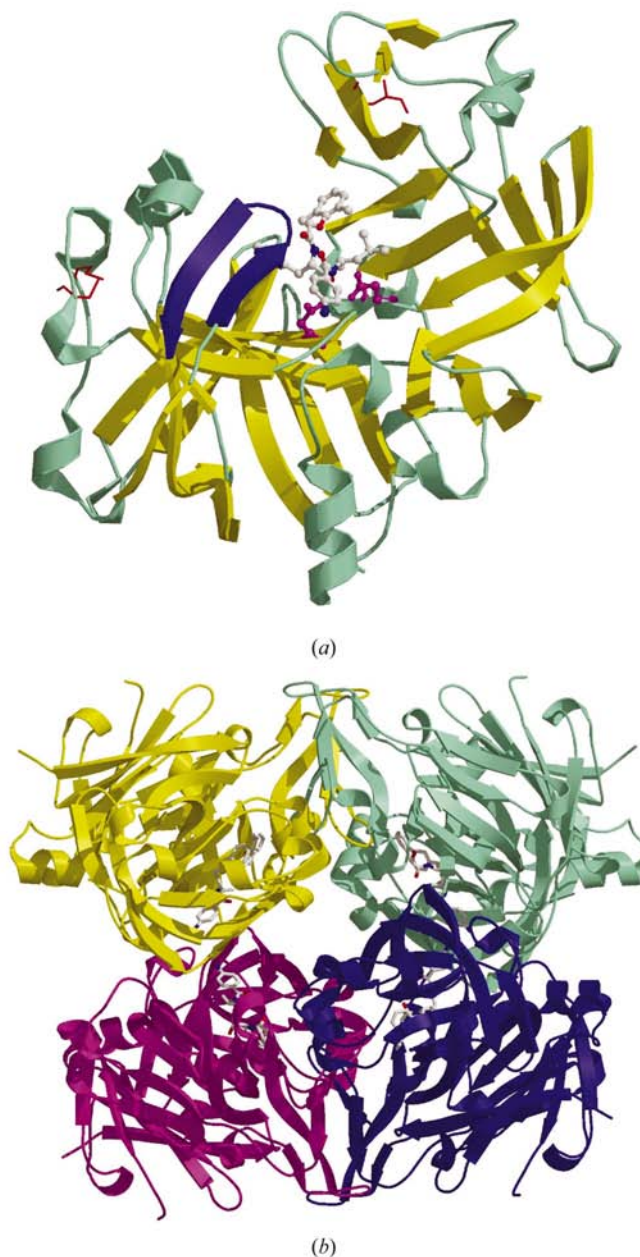

(a)

(b)

Figure 3
(a) Ribbon diagram of plasmepsin II in complex with rs370. Disulfide bridges are shown in red, the catalytic dyad in magenta, the inhibitor in gray and the flap in blue. (b) The tetramer of PMII–rs367 is generated along the two perpendicular twofold crystallographic axes of symmetry. The major dimer involves extensive interlocking of monomers and involves in one case the yellow and aquamarine monomers and in the other the magenta and blue monomers. The flexible loop of one monomer docks into the binding cavity of the other. The minor dimer is represented by the interactions along the other twofold axis of symmetry and involve in one case the yellow and magenta monomers and in the other the aquamarine and blue monomers. The interactions across this axis of symmetry are mediated by the proline-rich loop from one monomer, which comes into proximity to the binding cavity of the other.
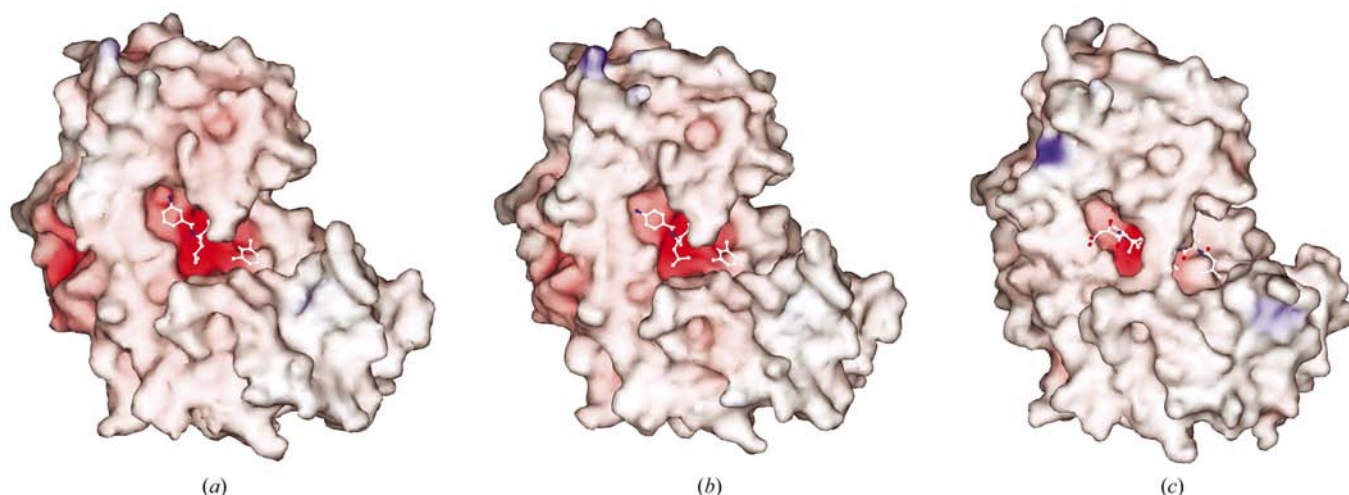

(a)

(b)

Figure 2
Two-dimensional representation of the chemical structure of inhibitors. (a) 3-amino-N-{4-[2-(2,6-dimethyl-phenoxy)-acetylamino]-3-hydroxy-1-isobutyl-5-phenylpentyl}-benzamide (rs367); (b) 4-amino-N-{4-[2-(2,6-dimethyl-phenoxy)-acetylamino]-3-hydroxy-1-isobutyl-5-phenylpentyl}-benzamide (rs370).

Figure 4
Surface plots of structures of PLM II in complex with (*a*) rs367, (*b*) rs370 and (*c*) pepstatin A. The protein surface is highly negatively charged and has two regions of positive charge. In addition, the binding cavity of the complex with pepstatin A is completely closed, while the other two are open.

1994). These values are quite low and suggest that the models are almost identical. The binding cavity is lined with water molecules, one of which assumes alternate positions depending on the position of the amino group and could be said to take the place of the amino group as it is moved from the 3′ to the 4′ position. The location of this water molecule is clearly defined in the $2F_o - F_c$ electron-density maps (Fig. 1).

The only difference between the inhibitors is the location of a single amino group on the P2′ group. The inhibitor rs370 is *para*-substituted, whereas rs367 is *meta*-substituted. As the inhibitors are so similar, it is not surprising that the resulting crystals are also very similar and have similar unit-cell parameters. They both crystallized in the same space group *I*222, with one monomer in the asymmetric unit. *I*222 symmetry generates a tetramer and there are three possible dimer interfaces. Two have significant buried areas, whereas the third has negligible buried area, 82 Å^2 in total. The major dimer interface has the largest total buried surface area, 4427 Å^2. The major dimer involves an extensive interlocking of the monomers along the crystallographic twofold (Fig. 3*b*). The greater proportion of the dimer interface is hydrophobic, 3455 Å^2, while a lesser proportion is hydrophilic, 852 Å^2. A loop region comprised of the residues Val236–Tyr245 forms a central part of the major crystallographic dimer interface and is in proximity to both the pro-loop and the flap. Furthermore, this loop from each monomer of the major dimer is in proximity to the inhibitor of the other monomer of the major dimer. The minor crystallographic dimer (Fig. 3*b*) has a total buried area of 1699 Å^2 and brings loop 290–297 of one monomer into proximity to the binding cavity of the other.

The major and minor crystallographic dimer interactions for the structure of the PLM II–rs367 complex are virtually identical to those of the structure of the PLM II–rs370 complex. The only difference between both structures is in minor dimer interactions at the active site, where there is now an additional hydrogen bond. Moving the amine from the *para* to the *meta* position brings it closer to the pro-loop of a symmetry-related monomer and leads to a 2.6 Å hydrogen bond between Pro295 and the amine group. No discernable gains have been observed from this additional hydrogen bond, as there is a negligible difference in the inhibition constants.

3.4. Comparison of complex structures of PLM II with RS367, RS370 and pepstatin A

Pepstatin A, rs367 and rs370 are presently three of the most potent inhibitors of PLM II. In the structures of PLM II

Figure 5
Overlay of the monomers of PLM II–pepstatin A (in yellow and magenta) with those of PLM II–rs367 and PLM II–rs370 (both in aquamarine) reveals that the binding cavity of PLM II–pepstatin A is more closed than that of the substrate-based inhibitors.

complexed with these inhibitors, the active site is flanked on one side by primarily hydrophobic residues and on the other side mostly by hydrophilic residues.

All three structural complexes have negatively charged surfaces with a net negative charge in the binding cavity (Fig. 4). There are two regions of positive charge on the surface of both structures, one of which is centralized around the highly variable flexible loop Val236–Tyr245. The flexible loop is the region of highest variability in eukaryotic aspartic proteases and adopts a different conformation with the Phe–Leu-based inhibitors than with pepstatin A (Fig. 5). The r.m.s. deviations of the overlap of the PLM II–rs367 and PLM II–rs370 complexes with the PLM II–pepstatin A complex model are 0.97 and 0.98 Å, respectively, for one monomer and 1.23 and 1.24 Å, respectively, for the second monomer. The regions of highest variability between the structures are the flexible loop and the binding cavity (Fig. 5).
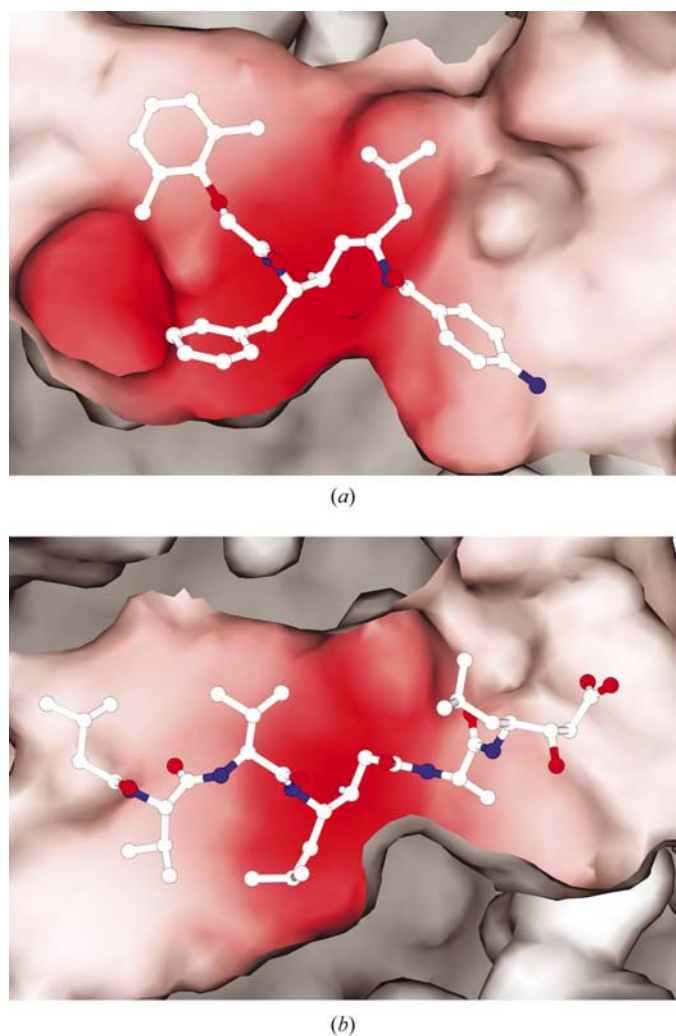
The binding cavities of the structures of both the PLM II–rs367 and PLM II–rs370 complexes are more open than that of the structure of the PLM II–pepstatin A complex. It appears that the extensive interactions within the binding pocket of the PLM II–pepstatin A complex results in a complete embrace of the inhibitor (Fig. 4b). Such a tight embrace of the inhibitor is quite unlike the more relaxed and open binding cavity of the other two structures. The conformational flexibility of the binding cavity is indicative of the need for more structural information to enhance structure-based drug-design studies and suggests that the complex structure of PLM II–pepstatin A is insufficient by itself for the thorough comprehension of the mode of binding of different classes of inhibitors. Furthermore, we have determined the structure of uncomplexed PLM II and the binding cavity is even more open than those of both the PLM II–rs367 and PLM II–rs370 complexes (Asojo et al., unpublished results). This suggests that the binding cavity starts out wider and more relaxed and closes down to embrace the different inhibitors that are bound.

A closer examination of the binding cavity of the PLM II–rs367 and PLM II–rs370 complexes reveals that the S1 and S1′ subsites conform well to accept the Phe and Leu residues (Fig. 6). It also becomes evident that there is sufficient room in the binding cavity for peptides of a much larger size than our inhibitors. In fact, it is possible to fit hemoglobin α-helix 21–36 into the binding cavity and at the same time the substrate residues Phe33 and Leu34 can be aligned with the corresponding inhibitor core (Fig. 7). There is no room for the hemoglobin α-helix to fit in the PLM II cavity in the conformation adopted when the inhibitor pepstatin A is bound
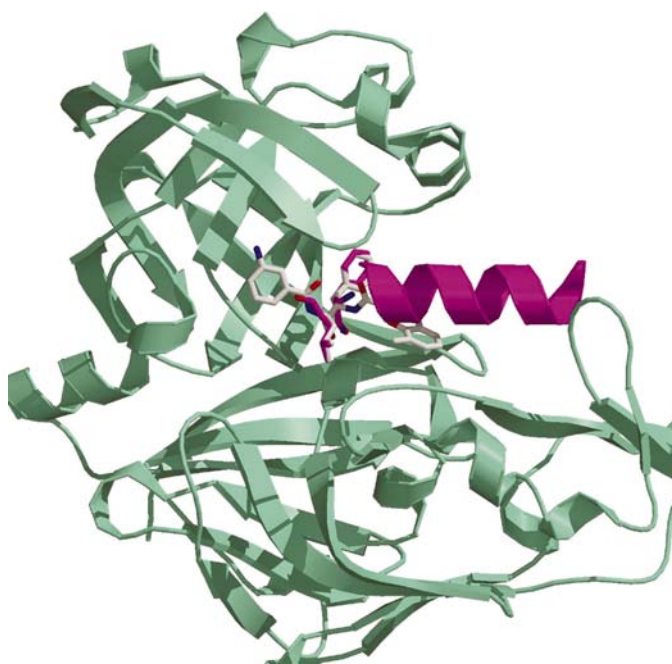

(a)

(b)

Figure 6
A closer look into the binding cavity of PLM II in complex with (a) rs370 and (b) pepstatin A. In the case of the latter, the cavity collapses completely as a result of the tight network of interactions with pepstatin A. The S1 and S1′ subsites of the former conform to accept the Phe and Leu residues and show a possible conformation of the binding cavity in the presence of the intended occupants.

Figure 7
The substrate helix (magenta) fits into the binding cavity of PLM II–rs370 (aquamarine). It is interesting to note that the Phe–Leu cleavage site of the substrate overlays well with the Phe–Leu core of the inhibitor.

(Fig. 5). This suggests that the relaxed conformation adopted by PLM II when either rs367 or rs370 are bound is more representative of the conformation of the substrate-bound enzyme than the conformation adopted when pepstatin A is bound.

There are fewer hydrogen bonds between the inhibitor rs370 and the binding cavity than observed in the PLM II–pepstatin A complex structure. This is as expected because rs370 is a smaller inhibitor with fewer hydrophilic groups than pepstatin A. Nonetheless, the hydrogen-bond contacts between the catalytic dyad are maintained at similar distances to those in the other complex structures (Fig. 8). Other conserved hydrogen bonds include those from the flap residues Val78 and Ser79, both of which are observed in the PLM II–pepstatin A complex structures. The hydrogen bond with Tyr192 is now reduced to a much weaker bond. There is also an additional hydrogen bond from Leu131 at a distance of 2.86 Å. This hydrogen bond is not observed in the PLM II–pepstatin A structure. The pattern of hydrogen bonding in the binding cavity of the structure of the PLM II–rs367 complex is virtually identical to that in the structure of the PLM II–rs370 complex.

3.5. Concluding remarks

Our structural studies indicate that there is significant conformational flexibility in the binding cavity of PLM II. To date, drug-design studies and modeling studies had relied on and utilized the conformational mode of PLM II when pepstatin A is bound as a structural basis for explaining inhibition results. This information is insufficient for the thorough examination, comprehension and prediction of the binding modes of different classes of inhibitors. Without an understanding of the multiple binding modes, incomplete and possibly inaccurate information will be derived from modeling studies. The conformational changes in the binding cavity provide new information that can be used in docking studies as well as structure-based drug-design studies on new classes of inhibitors. Further studies need to be carried out using the structural information in the design of more potent inhibitors with improved specificity for the plasmepsins.

3.6. Notes

All figures were generated using *Raster3D* (Merritt & Bacon, 1997), *MOLSCRIPT* (Kraulis, 1991) and *BOBSCRIPT* (Esnouf, 1997) except surfaces, which were generated using *SPOCK* (Christopher, 1998).
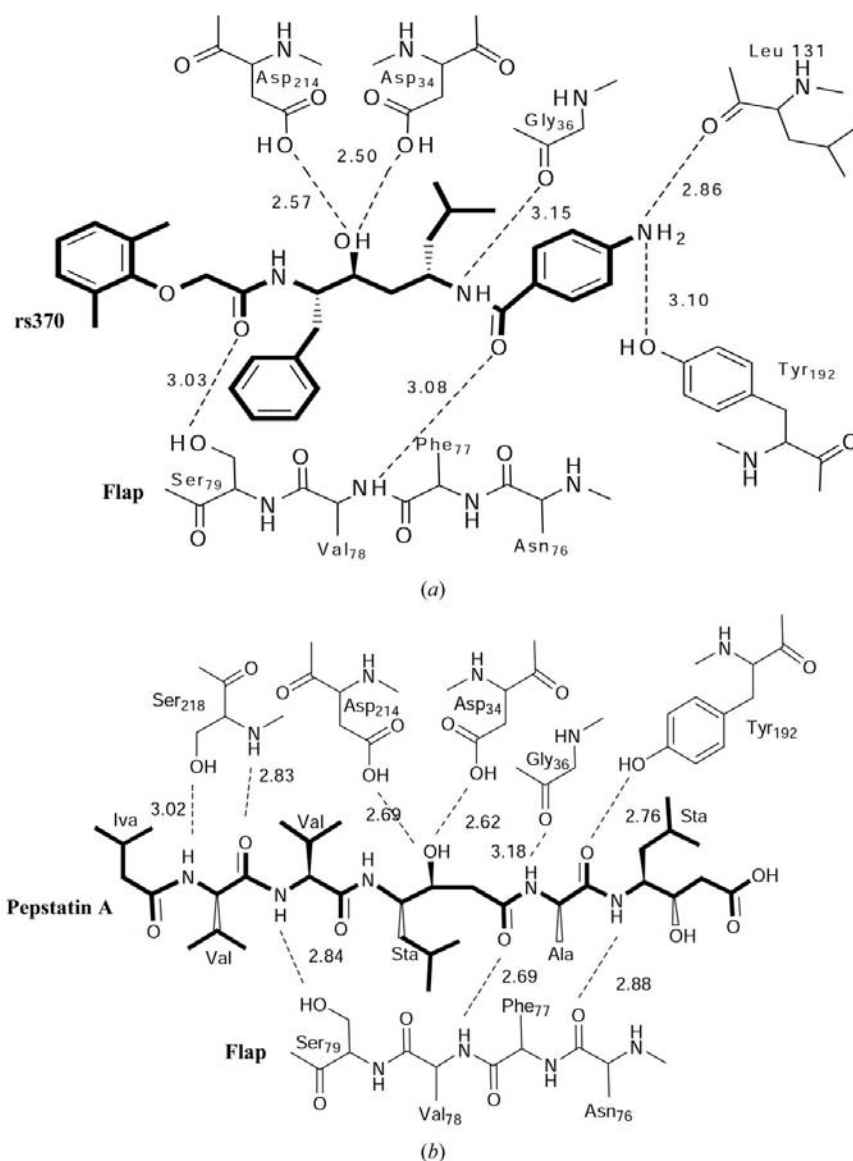

Figure 8
Comparison of the protein–ligand interactions across the active sites of plasmepsin II in complex with pepstatin A (*a*) and rs370 (*b*).

References

Adams, P. D., Pannu, N. S., Read, R. J. & Brünger, A. T. (1997). *Proc. Natl Acad. Sci. USA*, **94**, 5018–5023.
Banerjee, R., Liu, J., Beatty, W., Pelosof, L., Klemba, M. & Goldberg, D. E. (2002). *Proc. Natl Acad. Sci. USA*, **99**, 990–995.
Bernstein, N. K., Cherney, M. M., Loetscher, H., Ridley, R. G. & James, M. N. (1999). *Nature Struct. Biol.* **6**, 32–37.
Brünger, A. T. (1992*a*). *Nature (London)*, **355**, 472-474.
Brünger, A. T. (1992*b*). *X-PLOR: A System for X-ray Crystallography and NMR*. New Haven, CT, USA: Yale University Press.

Brünger, A. T., Adams, P. D. & Rice, L. M. (1997). *Structure*, **5**, 325–336.

Brünger, A. T., Krukowski, A. & Erickson, J. (1990). *Acta Cryst.* A**46**, 585–593.

Carroll, C. D., Johnson, T. O., Tao, S., Lauri, G., Orlowski, M., Gluzman, I. Y., Goldberg, D. E. & Dolle, R. E. (1998). *Bioorg. Med. Chem. Lett.* **8**, 3203–3206.

Carroll, C. D. & Orlowski, M. (1998). *Adv. Exp. Med. Biol.* **436**, 375–380.

Carroll, C. D., Patel, H., Johnson, T. O., Guo, T., Orlowski, M., He, Z. M., Cavallaro, C. L., Guo, J., Oksman, A., Gluzman, I. Y., Connelly, J., Chelsky, D., Goldberg, D. E. & Dolle, R. E. (1998). *Bioorg. Med. Chem. Lett.* **8**, 2315–2320.

Christopher, J. A. (1998). *SPOCK: The Structural Properties Observations and Calculation Kit.* The Center for Macromolecular Design, Texas A&M University, College Station, TX, USA.

Collaborative Computational Project, Number 4 (1994). *Acta Cryst.* D**50**, 760–763.

Dame, J. B., Reddy, G. R., Yowell, C. A., Dunn, B. M., Kay, J. & Berry, C. (1994). *Mol. Biochem. Parasitol.* **64**, 177–190.

Esnouf, R. M. (1997). *J. Mol. Graph. Model.* **15**, 132–134.

Francis, S. E., Gluzman, I. Y., Oksman, A., Banerjee, D. & Goldberg, D. E. (1996). *Mol. Biochem. Parasitol.* **83**, 189–200.

Francis, S. E., Gluzman, I. Y., Oksman, A., Knickerbocker, A., Mueller, R., Bryant, M. L., Sherman, D. R., Russell, D. G. & Goldberg, D. E. (1994). *EMBO J.* **13**, 306–317.

Francis, S. E., Sullivan, D. J. Jr & Goldberg, D. E. (1997). *Annu. Rev. Microbiol.* **51**, 97–123.

Gluzman, I. Y., Francis, S. E., Oksman, A., Smith, C. E., Duffin, K. L. & Goldberg, D. E. (1994). *J. Clin. Invest.* **93**, 1602–1608.

Goldberg, D. E. (1992). *Infect. Agents Dis.* **1**, 207–211.

Goldberg, D. E., Slater, A. F., Beavis, R., Chait, B., Cerami, A. & Henderson, G. B. (1991). *J. Exp. Med.* **173**, 961–969.

Gulnik, S. V., Afonina, E. I., Gustchina, E., Yu, B., Silva, A. M., Kim, Y. & Erickson, J. W. (2002). *Protein Expr. Purif.* **24**, 412–419.

Haque, T. S., Skillman, A. G., Lee, C. E., Habashita, H., Gluzman, I. Y., Ewing, T. J., Goldberg, D. E., Kuntz, I. D. & Ellman, J. A. (1999). *J. Med. Chem.* **42**, 1428–1440.

Jones, T. A., Zou, J. Y., Cowan, S. W. & Kjeldgaard, M. (1991). *Acta Cryst.* A**47**, 110–119.

Kabsch, W. (1976). *Acta Cryst.* A**32**, 922–923.

Kraulis, P. J. (1991). *J. Appl. Cryst.* **24**, 946–950.

Laskowski, R. A., MacArthur, M. W., Moss, D. S. & Thornton, J. M. (1993). *J. Appl. Cryst.* **26**, 283–291.

Merritt, E. A. & Bacon, D. J. (1997). *Methods Enzymol.* **277**, 505–524.

Navaza, J. (1994). *Acta Cryst.* A**50**, 157–163.

Otwinowski, Z. (1993a). *DENZO: An Oscillation Data Processing Program for Macromolecular Crystallography.* New Haven, CT, USA: Yale University Press.

Otwinowski, Z. (1993b). *SCALEPACK: Software for the Scaling Together of Integrated Intensities Measured on a Number of Separate Diffraction Images.* New Haven, CT, USA: Yale University Press.

Rosenthal, P. J., Wollish, W. S., Palmer, J. T. & Rasnick, D. (1991). *J. Clin. Invest.* **88**, 1467–1472.

Semenov, A., Olson, J. E. & Rosenthal, P. J. (1998). *Antimicrob. Agents Chemother.* **42**, 2254–2258.

Silva, A. M., Lee, A. Y., Erickson, J. W. & Goldberg, D. E. (1998). *Adv. Exp. Med. Biol.* **436**, 363–373.

Silva, A. M., Lee, A. Y., Gulnik, S. V., Maier, P., Collins, J., Bhat, T. N., Collins, P. J., Cachau, R. E., Luker, K. E., Gluzman, I. Y., Francis, S. E., Oksman, A., Goldberg, D. E. & Erickson, J. W. (1996). *Proc. Natl Acad. Sci. USA*, **93**, 10034–10039.

Westling, J., Cipullo, P., Hung, S. H., Saft, H., Dame, J. B. & Dunn, B. M. (1999). *Protein Sci.* **8**, 2001–2009.

World Health Organization (1995). In *Control of Tropical Diseases: Malaria Control.* Geneva, Switzerland: WHO Office of Information.